

Late-time X-ray Observations of the Jetted Tidal Disruption Event AT2022cmc: The Relativistic Jet Shuts Off

T. EFTEKHARI,^{1,*} A. TCHEKHOVSKOY,¹ K. D. ALEXANDER,² E. BERGER,³ R. CHORNOCK,⁴ T. LASKAR,⁵ R. MARGUTTI,^{4,6}
Y. YAO,^{4,7} Y. CENDES,^{8,3} S. GOMEZ,⁹ A. HAJELA,¹⁰ AND D. R. PASHAM¹¹

¹Center for Interdisciplinary Exploration and Research in Astrophysics (CIERA) and Department of Physics and Astronomy, Northwestern University, Evanston, IL 60208, USA

²Department of Astronomy and Steward Observatory, University of Arizona, 933 North Cherry Avenue, Tucson, AZ 85721-0065, USA

³Center for Astrophysics | Harvard & Smithsonian, 60 Garden St, Cambridge, MA 02138, USA

⁴Department of Astronomy, University of California, Berkeley, CA 94720-3411, USA

⁵Department of Physics & Astronomy, University of Utah, Salt Lake City, UT 84112, USA

⁶Department of Physics, University of California, 366 Physics North MC 7300, Berkeley, CA 94720, USA

⁷Miller Institute for Basic Research in Science, 468 Donner Lab, Berkeley, CA 94720, USA

⁸Department of Physics, University of Oregon, Eugene, OR 97403, USA

⁹Space Telescope Science Institute, 3700 San Martin Dr, Baltimore, MD 21218, USA

¹⁰DARK, Niels Bohr Institute, University of Copenhagen, Niels Bohr Building (NBB), Jagtvej 155A, 1. floor, 2200 Copenhagen N., Denmark

¹¹Kavli Institute for Astrophysics and Space Research, Massachusetts Institute of Technology, Cambridge, MA 02139, USA

ABSTRACT

The tidal disruption event (TDE) AT2022cmc represents the fourth known example of a relativistic jet produced by the tidal disruption of a stray star providing a unique probe of the formation and evolution of relativistic jets in otherwise dormant supermassive black holes (SMBHs). Here we present deep, late-time *Chandra* observations of AT2022cmc extending to $t_{\text{obs}} \approx 400$ days after disruption. Our observations reveal a sudden decrease in the X-ray brightness by a factor of $\gtrsim 14$ over a factor of ≈ 2.3 in time, and a deviation from the earlier power-law decline with a steepening $\alpha \gtrsim 3.2$ ($F_X \propto t^{-\alpha}$), steeper than expected for a jet break, and pointing to the cessation of jet activity at $t_{\text{obs}} \approx 215$ days. Such a transition has been observed in two previous TDEs (*Swift* J1644+57 and *Swift* J2058+05). From the X-ray luminosity and the timescale of jet shutoff, we parameterize the mass of the SMBH in terms of unknown jet efficiency and accreted mass fraction parameters. Motivated by the disk-jet connection in AGN, we favor black hole masses $\lesssim 10^5 M_{\odot}$ (where the jet and disk luminosities are comparable), and disfavor larger black holes (in which extremely powerful jets are required to outshine their accretion disks). We additionally estimate a total accreted mass of $\approx 0.1 M_{\odot}$. Applying the same formalism to *Swift* J1644+57 and *Swift* J2058+05, we favor comparable black hole masses for these TDEs of \lesssim a few $\times 10^5 M_{\odot}$, and suggest that jetted TDEs may preferentially form from lower mass black holes when compared to non-relativistic events, owing to generally lower jet and higher disk efficiencies at higher black hole masses.

Keywords: Tidal disruption events; relativistic jets; accretion disks; transients

1. INTRODUCTION

The tidal disruption of a stray star by a supermassive black hole (SMBH) offers a unique opportunity to study the full life-cycle of jets and outflows powered by black holes (Giannios & Metzger 2011; De Colle & Lu 2020; Dai et al. 2021). Indeed, a small fraction of tidal disruption events (TDEs) discovered to date have been found to harbor powerful relativistic jets (Bloom et al. 2011; Burrows et al. 2011; Levan et al. 2011; Zauderer et al. 2011; Cenko et al. 2012; Brown et al. 2015; Andreoni et al. 2022a; Pasham et al. 2023). The precise mechanisms governing the production and evolution

of jets in TDEs are poorly understood, although prevailing theories invoke jet launching via the Blandford-Znajek (BZ) mechanism (Blandford & Znajek 1977) in which spin energy is extracted from a rapidly spinning black hole through large-scale magnetic fields (Tchekhovskoy et al. 2014; Kelley et al. 2014). However, the reservoir of magnetic flux available for producing such strong magnetic fields in otherwise quiescent systems (e.g., from the disrupted star or a pre-existing fossil accretion disk) remains an open question (e.g., Kelley et al. 2014; Guillochon & McCourt 2017; Bonnerot et al. 2017).

The discovery of two γ -ray transients by the *Swift*/Burst Alert Telescope (BAT) in 2011 provided the first unambiguous cases of relativistic jets in TDEs (Levan et al. 2011; Burrows et al. 2011; Bloom et al. 2011; Zauderer et al.

* NHFP Einstein Fellow

2011; Cenko et al. 2012). Following their discoveries, *Swift* J164449.3+573451 (hereafter Sw J1644+57) and *Swift* J2058.4+0516 (hereafter Sw J2058+05) were localized to the nuclei of distant galaxies at $z = 0.354$ and $z = 1.1853$ respectively, and were notably similar in their early time behavior in the radio, infrared, and X-ray bands. In both cases, the early X-ray emission exhibited rapid variability on timescales as short as $\lesssim 500$ seconds (Brown et al. 2015; Mangano et al. 2016), and X-ray luminosities several orders of magnitude above the Eddington limit for a $\sim 10^6 M_\odot$ black hole, below the maximum allowed mass of $\sim 10^8 M_\odot$ for TDE flares. For Sw J1644+57, the discovery of bright radio-to-millimeter synchrotron emission independently established the presence of a collimated relativistic jet with a Lorentz factor of $\Gamma \sim \text{few}$ (Zauderer et al. 2011; Berger et al. 2012). Sw J1644+57's X-ray luminosity subsequently declined following roughly a $t^{-5/3}$ power law decay (Mangano et al. 2016), as expected for fallback accretion in a TDE (Rees 1988), while Sw J2058+05 had a steeper decay with $t^{-2.2}$. A third jetted TDE, *Swift* J1112.2–8238 (hereafter Sw J1112–82; $z = 0.89$), was discovered in June 2011 (Brown et al. 2015), although limited data are available for this event.

A remarkable feature of the first two jetted TDEs is a sudden drop in their X-ray light curves at late times, marking a fundamental change in the nature of the X-ray emission. Deep *XMM-Newton* and *Chandra* follow-up observations of Sw J1644+57 showed a precipitous decline in the X-ray luminosity by a factor of ≈ 170 beginning about $t_{\text{rest}} \sim 370$ days after the discovery and over a timescale of only ~ 70 days (Zauderer et al. 2013). For Sw J2058+05, the X-ray luminosity declined by a factor of ~ 160 at $t_{\text{rest}} \sim 250$ days over a similar span of $\lesssim 70$ days (Pasham et al. 2015). In the case of Sw J1112–82, a sharp decline in the X-ray flux was observed at $t_{\text{rest}} \sim 20$ days, followed by a non-detection at ~ 500 days, although this is not inconsistent with the order of magnitude variability observed in the X-ray light curve for Sw J1644+57 (Saxton et al. 2012). The sudden decrease in X-ray flux observed for Sw J1644+57 and Sw J2058+05 has been attributed to the cessation of jet activity as the accretion state transitions from super- to sub-Eddington accretion (Zauderer et al. 2013; Pasham et al. 2015), providing novel constraints on the properties of the disrupted star and SMBH (Tchekhovskoy et al. 2014).

Over a decade since the discoveries of the first jetted TDEs, observations have revealed that relativistic jets in TDEs are extremely rare (Alexander et al. 2020). Compared to the rate of non-jetted TDEs ($\sim 10^3 \text{ Gpc}^{-3} \text{ yr}^{-1}$; Stone et al. 2020), TDEs that appear to power on-axis relativistic jets comprise less than 1% of the TDE population (Sun et al. 2015; Andreoni et al. 2022a), suggesting that such events may require special conditions (e.g., high black hole spins or a strong magnetic flux threading the black hole; Tchekhovskoy et al. 2014)

or implicate viewing angle effects in which the majority of jets are beamed out of our line of sight. Indeed, the emergence of delayed radio emission from a subset of TDEs (e.g., Horesh et al. 2021a; Cendes et al. 2023) can potentially be explained by off-axis jets (Sfaradi et al. 2024; Sato et al. 2024), though non-relativistic outflows provide a viable mechanism as well. Nonetheless, the fraction of powerful jets similar to Sw J1644+57 still appears to be extremely small. The apparent diversity in the X-ray spectra of jetted and non-jetted TDEs (Auchettl et al. 2018), with the former exhibiting generally harder X-ray emission, may be naturally reconciled by the observer's viewing angle with respect to the accretion disk (Dai et al. 2018). Alternatively, a misalignment between the black hole spin axis and orbital plane of the star may produce a quasi-spherical outflow that prevents all but the most powerful and highly magnetized jets from escaping, leading to the observed dichotomy (Lu et al. 2023; Teboul & Metzger 2023).

The discovery of the relativistic TDE AT2022cmc on 2022 February 11 by the Zwicky Transient Facility (ZTF) marked the first jetted TDE discovered in the optical and the first observed to launch a relativistic jet in the last decade. Unlike the *Swift*-detected events, AT2022cmc was initially discovered as a fast-fading optical transient (Andreoni et al. 2022b). Subsequent spectroscopic observations identified a redshift of $z = 1.193$ (Tanvir et al. 2022), heralding AT2022cmc as the furthest TDE discovered to date. The early time X-ray emission from AT2022cmc was highly variable (Pasham et al. 2023), similar to the early X-ray light curve of Sw J1644+57, and was interpreted as synchrotron radiation due to energy dissipation within a magnetically dominated jet (Yao et al. 2024). Observations at radio and submillimeter wavelengths further supported the presence of a relativistic jet expanding into an ambient medium (Andreoni et al. 2022a; Pasham et al. 2023; Rhodes et al. 2023), as with Sw J1644+57.

As one of a small sample of jetted TDEs, AT2022cmc affords a rare opportunity to gain insight into the emission mechanism operating in the accretion disk at early times (Pasham et al. 2023; Yao et al. 2024), as well as the properties of the SMBH and disrupted star through long-term monitoring of the X-ray light curve. Here we present late-time *Chandra* X-ray observations of AT2022cmc. Proceeding under the assumption that the X-ray emission from AT2022cmc is dominated by a relativistic jet, our observations demonstrate that the jet has shut off at $t_{\text{rest}} \sim 100$ days, as evidenced by a sudden drop in the X-ray luminosity and a deviation from an earlier power-law decline. The X-ray data allow us to uniquely probe the mass of the disrupting SMBH and the total accreted mass. We adopt the discovery epoch MJD 59621.4463 (2022 February 11 at 10:42:40 UTC) as the reference epoch. Throughout the paper, we use the Planck cosmological parameters for a flat

Table 1. *Chandra* X-ray Observations of AT2022cmc

Observation Epoch (MJD)	Exposure Time (ks)	$t_{\text{obs}}^{\text{a}}$ (days)	$t_{\text{rest}}^{\text{b}}$ (days)	Net Count Rate (0.5–8 keV) (cts s ⁻¹)	Flux ^c (0.3–10 keV) (erg cm ⁻² s ⁻¹)
2023 Feb 24	30.17	378	172	$< 2.19 \times 10^{-4}$	$< 4.16 \times 10^{-15}$
2023 Mar 28	15.37	410	187	$< 4.30 \times 10^{-4}$	$< 8.16 \times 10^{-15}$
2023 Mar 29	44.58	411	187	$< 1.48 \times 10^{-4}$	$< 2.81 \times 10^{-15}$
2023 Mar 18 ^d	90.12	400	182	$< 7.33 \times 10^{-5}$	$< 1.39 \times 10^{-15}$

NOTE—Limits correspond to 3σ .

^a Observer frame.

^b Rest-frame.

^c Absorbed flux.

^d Average exposure-weighted observation epoch corresponding to merged observation.

Λ CDM universe, with $H_0 = 67.66 \text{ km s}^{-1} \text{ Mpc}^{-1}$, $\Omega_m = 0.310$, and $\Omega_\lambda = 0.690$ (Planck Collaboration et al. 2020).

2. CHANDRA X-RAY OBSERVATIONS

We obtained three epochs of X-ray observations of AT2022cmc with the *Chandra* Advanced CCD Imaging Spectrometer (ACIS-S; Obs IDs: 26791, 26792, 27769; PI: Eftekhari)¹ on UT 2023 February 24, March 28, and March 29 with a total exposure time of 90.12 ks. Details of the observations and individual exposure times are given in Table 1. We analyze the data using the CIAO software package (v4.13), following standard ACIS data filtering. We do not detect X-ray emission at the position of AT2022cmc using `wavdetect` in any of the individual epochs. We align the individual epochs to a common astrometric solution using `wcs_match` and `wcs_update` and sources identified in our longest exposure image (Obs ID: 27769) using `wavdetect` as a reference. We then merge the observations to generate a co-added, exposure-corrected image using `merge_obs`. We do not detect any counts in a 1'' radius aperture centered at the position of AT2022cmc in the merged event file, corresponding to a 3σ upper limit on the 0.5–8 keV count rate of $7.3 \times 10^{-5} \text{ cts s}^{-1}$ (assuming Poisson statistics; Gehrels 1986). Adopting a photon index of $\Gamma = 1.6$ (the best fit photon index from fits to *Swift*/XRT data²; Pasham et al. 2023), $N_{\text{H,MW}} = 8.8 \times 10^{19} \text{ cm}^{-2}$ (Kalberla et al. 2005), and $N_{\text{H,int}} = 10^{21} \text{ cm}^{-2}$ (Yao et al. 2024), the 3σ limit on the observed 0.3–10 keV absorbed X-ray flux³ is $F_X \lesssim 1.39 \times 10^{-15} \text{ erg cm}^{-2} \text{ s}^{-1}$. We note that the X-ray spectrum of AT2022cmc is consistent with synchrotron emission

from a magnetically dominated jet (Yao et al. 2024), similar to that of Sw J1644+57 (Burrows et al. 2011).

We plot our X-ray limits for AT2022cmc, including our merged limit (with an average exposure-weighted observation epoch of $t_{\text{rest}} \approx 182$ days post-disruption) and limits for individual epochs in Figure 1. We also plot X-ray data collected by *Swift*/XRT between MJD 59633 and MJD 59810 ($t_{\text{rest}} \sim 5–86$ days) as compiled in Yao et al. 2024 and data from *XMM-Newton* (with a best fit photon index $\Gamma = 1.65$; Yao et al. 2024), including a detection and upper limit at $t_{\text{rest}} \sim 52$ and 137 days, respectively. We note that based on experience, the *Chandra*/ACIS-S vs. *Swift*/XRT inter-calibration should impart negligible variations to the light curve of order $< 15\%$.

3. RESULTS

3.1. The Relativistic Jet Shuts Off

The X-ray light curve of AT2022cmc (Figure 1) exhibits rapid ($\sim 10^3 \text{ s}$) variability on timescales of \sim weeks after its initial discovery (Pasham et al. 2023) and an overall $F_X \propto t^{-1.9}$ decline to $t_{\text{rest}} \approx 80$ days. The $t^{-1.9}$ decline is somewhat steeper than the canonical $t^{-5/3}$ decay for TDEs and may be indicative of a partial stellar disruption in which the stellar core survives and is able to partially oppose the black hole’s gravitational force (Guillochon & Ramirez-Ruiz 2013). In particular, the deviation from $t^{-5/3}$ on the observed timescale of $t_{\text{rest}} \lesssim 100$ days may imply a substantial stellar core in which $\gtrsim 15\%$ of the initial stellar mass is left behind (Coughlin & Nixon 2019). Our deep *Chandra* limit at $t_{\text{rest}} \sim 182$ days indicates a decrease in the X-ray flux by a factor of $\gtrsim 14$ and a deviation from the earlier power-law decline with a steepening $\alpha \gtrsim 3.2$ ($F_X \propto t^{-\alpha}$) pointing to a change in the nature of the X-ray emission,⁴ which we attribute to the cessation of jet activity.

¹ This paper employs a list of *Chandra* datasets, obtained by the *Chandra* X-ray Observatory, contained in DOI: 266.

² There is minimal evolution in the *Swift*/XRT X-ray spectrum at $t_{\text{rest}} \sim 2–10$ days, with the best fit photon index varying between $\Gamma \sim 1.3–1.9$.

³ <https://cxc.harvard.edu/toolkit/pimms.jsp>

⁴ We note that the steepening in the X-ray light curve is inconsistent with a jet break for which we expect a shallower power-law index (Sari et al. 1999; Wang et al. 2018).

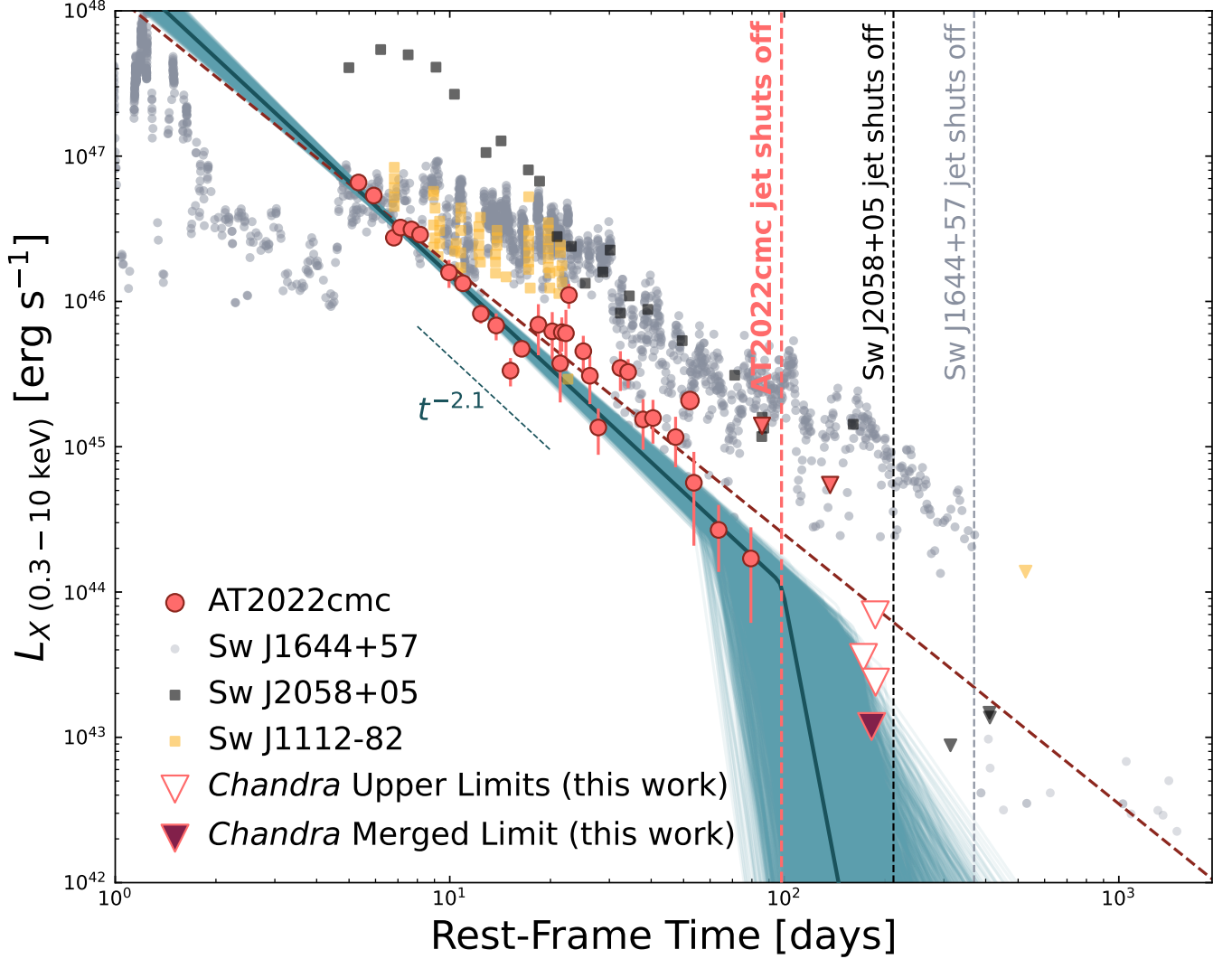


Figure 1. Stringent late-time upper limits on the X-ray emission of AT2022cmc obtained in this work place robust constraints on the shut-off time of the relativistic jet. Our late-time *Chandra* observations (large open triangles) and our merged *Chandra* epoch (large solid triangle) at $t_{\text{rest}} \approx 182$ days indicate a deviation from the earlier power-law decline (dashed maroon line) in the X-ray light curve based on *Swift*/XRT ($t_{\text{rest}} \sim 5\text{--}86$ days; Yao et al. 2024) and *XMM-Newton* ($t_{\text{rest}} = 52$ and 137 days; Yao et al. 2024) data. Our best fit broken power-law model is shown as a dark blue line, while light blue lines represent random samples from the MCMC chains. Also shown for comparison are the X-ray light curves of other jetted TDEs, including Sw J1644+57 (light gray circles; Burrows et al. 2011; Zauderer et al. 2013; Eftekhari et al. 2018), Sw J2058+05 (dark gray squares; Pasham et al. 2015), and Sw J1112-82 (yellow squares; Brown et al. 2015). Vertical dashed lines indicate the time of jet shut-off for each event.

To quantify this, we fit a smoothed broken power-law of the form

$$F_X(t) = F_X \left[\left(\frac{t}{t_{\text{off}}} \right)^{-s\alpha_1} + \left(\frac{t}{t_{\text{off}}} \right)^{-s\alpha_2} \right]^{-1/s} \quad (1)$$

to the X-ray light curve using *emcee* (Foreman-Mackey et al. 2013), a Python-based implementation of a Markov Chain Monte Carlo (MCMC) Ensemble Sampler. We fix the smoothing parameter $s = 10$ and fit for the break point t_{off} , the flux normalization F_X at t_{off} , and the power-law indices before (α_1) and after (α_2) the break, and include an additional parameter

which accounts for an underestimate of the variance in the light curve by a constant factor f .

To incorporate the upper limits into the fits, we adopt the prescription from Laskar et al. (2014) in which the likelihood function accounts for both detections and non-detections in a given data set and is given by (Lawless 2002; Helsel 2005):

$$\mathcal{L} = \prod p(e_i)^{\delta_i} F(e_i)^{(1-\delta_i)} \quad (2)$$

where e_i are the residuals between the predicted model flux and the measurement or 3σ upper limit, $p(e_i)$ and $F(e_i)$ are the probability density and cumulative distribution functions

of the residuals, respectively, and δ_i indicates an upper limit ($\delta_i = 0$) or a detection ($\delta_i = 1$). We approximate the measurement uncertainties (σ_i) as Gaussian by taking the mean of the asymmetric errors on each data point and adopt for the non-detections the Poisson single-sided upper limits. The probability density and cumulative distribution functions are therefore given by

$$p(e_i) = \frac{1}{\sqrt{2\pi}\sigma} \exp^{-e_i^2/2\sigma^2} \quad (3)$$

and

$$F(e_i) = \frac{1}{2} \left[1 + \operatorname{erf} \left(\frac{e_i}{\sqrt{2}\sigma_i} \right) \right], \quad (4)$$

respectively, where erf is the error function.

For the priors, we use log-uniform priors for F_X and t_{off} , fixing the allowed range for t_{off} to span the full timescale of the X-ray light curve ($t_{\text{rest}} \sim 0 - 200$ days) and allowing for a possible break at earlier times as evidenced by an apparent steepening at $t_{\text{rest}} \approx 50$ d (see Figure 1). We use linearly uniform priors for both power-law indices with $-5 < \alpha_1 < 0$ and $-15 < \alpha_2 < -3.2$, where the upper bound on α_2 is set by the slope between the last *Swift*/XRT detection and our deep *Chandra* upper limit. The posterior distributions are sampled using 1000 Markov chains and 95000 steps, where we discard the first 10000 steps ($\approx 10 \times$ the integrated autocorrelation length) to ensure the walkers have sufficiently converged and that the samples represent independent, uncorrelated measures of the target distribution. We further assess the quality of our MCMC samples by calculating the acceptance fraction of the ensemble and find a mean acceptance fraction of 0.22, within the nominally accepted range (Gelman et al. 1996). The best fit parameters and posterior distributions are given in Table 2 and Figure 2, respectively.

Based on the results of our MCMC analysis, we find evidence for a break in the X-ray light curve at $t_{\text{off}} \equiv t_{\text{rest}} = 98^{+38}_{-26}$ days ($t_{\text{obs}} \approx 215$ days). We note a degeneracy between the jet shut-off time t_{off} and the flux normalization F_X given the sparse temporal coverage in the light curve between the last detection and our late-time *Chandra* limits. Compared to Sw J2058+05 and Sw J1644+57, the two known jetted TDEs with observed X-ray drop-offs at $t_{\text{rest}} \approx 200$ and 370 days, respectively, the drop in AT2022cmc’s X-ray light curve occurs a factor of two to four times earlier. We explore the implications of this in Section 3.3.

3.2. Estimating the Mass of the Disrupting SMBH: X-ray Luminosity

The abrupt decrease in the X-ray luminosity at $t_{\text{rest}} \approx 100$ days for AT2022cmc can be interpreted as an accretion state transition from super- to sub-Eddington, providing a novel estimate for the mass of the disrupting SMBH. Such a transition is predicted from numerical simulations as the accretion

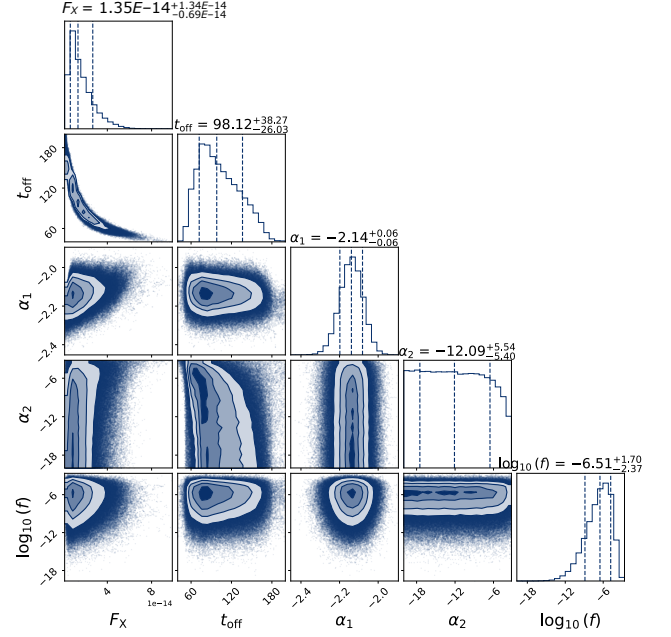


Figure 2. Results from our MCMC parameter estimation for a broken power law fit to the X-ray light curve of AT2022cmc. Marginalized posterior distributions for each parameter are shown on the diagonal, where dashed lines indicate the median and 68% confidence interval.

disk becomes geometrically thin and radiatively efficient (De Colle et al. 2012). Here we leverage the observational data for AT2022cmc to estimate the mass of the disrupting SMBH.

To first order, we can estimate M_{BH} by equating the X-ray luminosity at turnoff to the Eddington luminosity. Assuming the jet shuts off at an Eddington ratio $\lambda = \dot{M}/\dot{M}_{\text{Edd}} = 1$ ($\dot{M}_{\text{Edd}} = L_{\text{Edd}}/\epsilon_{\text{disk}}c^2$), the disk luminosity at shut-off ($L_{\text{disk,off}} = \epsilon_{\text{disk}}\dot{M}_{\text{BH}}c^2$) is equal to the Eddington luminosity, and we can therefore parameterize the black hole mass as

$$M_{\text{BH}} = 10^5 \frac{L_{\text{jet,off}}}{1.19 \times 10^{45} \text{ erg s}^{-1}} \left(\frac{\epsilon_{\text{disk}}}{\epsilon_{\text{jet}}} \right) f_{\text{beam},200}^{-1} f_{\text{bol},3} M_{\odot} \quad (5)$$

where $L_{\text{jet,off}} = \epsilon_{\text{jet}}\dot{M}_{\text{BH}}c^2$ is the isotropic X-ray luminosity at jet shut-off and is equal to $L_{\text{disk,off}}(\epsilon_{\text{jet}}/\epsilon_{\text{disk}})$ for $\lambda = 1$, and ϵ_{jet} and ϵ_{disk} are the jet and disk radiative efficiencies, respectively. We convert the observed isotropic X-ray luminosity $L_{\text{jet,off}}$ into an intrinsic jet luminosity L_{jet} for a “standard” jet assuming a relativistic beaming correction $f_{\text{beam}} = 200f_{\text{beam},200}$ for a beaming angle of 0.1 rad (as estimated for Sw J1644+57) and a bolometric correction $f_{\text{bol}} = 3f_{\text{bol},3}$ (as in previous work for jetted TDEs; Burrows et al. 2011; Pasham et al. 2015) to increase the observed X-ray luminosity by a factor of 3.

In Figure 3, we plot $\eta_{\text{jet}} \equiv \epsilon_{\text{jet}}/\epsilon_{\text{disk}}$ as a function of M_{BH} using equation 5 where we set $L_{\text{jet,off}}$ equal to the break luminosity at the time of jet shut-off from our MCMC fit ($L_X \approx 10^{44} \text{ erg s}^{-1}$). The result is a curve in the $\eta_{\text{jet}} - M_{\text{BH}}$ parameter

Table 2. AT2022cmc X-ray Light curve Broken Power Law Fit

Parameter	Best Fit
F_X (0.3–10 keV) ($\text{erg cm}^{-2} \text{s}^{-1}$)	$1.35_{-0.7}^{+1.3} \times 10^{-14}$
t_{off}^a (d)	98_{-26}^{+38}
α_1	$-2.1_{-0.1}^{+0.1}$
α_2	$-12.1_{-5.4}^{+5.5}$

NOTE—^aRest-frame time.

space, corresponding to the ratio of intrinsic⁵ jet and disk luminosities at jet shut-off ($\eta_{\text{jet}} \equiv L_{\text{jet,off}}/f_{\text{beam},200}^{-1}f_{\text{bol},3}/L_{\text{disk,off}}$). We repeat the above exercise for Sw J1644+57 and Sw J2058+05, the two other jetted TDEs with observed X-ray drop-offs, and plot the results in Figure 3. For Sw J2058+05, we re-fit the X-ray light curve to better constrain t_{off} (see Appendix A). In each case, the width of the curve corresponds to the uncertainty in the X-ray luminosity at jet shut-off.

Studies of the disk-jet connection in AGN, including the most powerful blazars, indicate that the power in relativistic jets is strongly coupled to their accretion disk luminosities (Ghisellini et al. 2010; Inoue et al. 2017). The intrinsic power radiated by the jet in the form of non-thermal luminosity (a factor of at least 3–10 times smaller than the jet’s bulk kinetic power) is quite large, and in some cases equal to, or only a factor of a few times smaller than the disk luminosity (Ghisellini et al. 2010). Moreover, theoretical work investigating accretion dynamics and jet power in relativistic TDEs has shown that the jet power exceeds the disk luminosity for reasonable system parameters⁶ (Piran et al. 2015), and particularly at lower black hole masses (Krolik & Piran 2012). Thus motivated, we favor values of $\eta_{\text{jet}} \gtrsim 10^{-1}$ for AT2022cmc where the disk and jet luminosities are comparable, and hence black hole masses $\lesssim 10^5 M_{\odot}$. We note that our inference of a high jet efficiency is furthermore consistent with the high jet efficiency inferred for AT2022cmc in the unified TDE framework of Teboul & Metzger (2023) based on the early X-ray peak which implies a promptly escaping jet and rapid magneto-spin alignment with the SMBH spin. We find similar results for both Sw J1644+57 and Sw J2058+05, which exhibit comparable X-ray luminosities at jet shut-off, where $M_{\text{BH}} \lesssim$ a few $\times 10^5 M_{\odot}$ for $\eta_{\text{jet}} \gtrsim 10^{-1}$. We note that larger black hole masses ($\sim 10^7 M_{\odot}$) are disfavored, as these would imply that the jet power is suppressed well below the luminosity of the accretion flow, which we consider contrived, particularly in

⁵ Here we consider the intrinsic jet luminosity as an approximation for a “standard” jet with $\theta_j \sim 0.1$ rad given the unknown jet opening angle.

⁶ This analysis assumes a low radiative disk efficiency ($\epsilon_{\text{disk}} = 0.057$) while at jet shut-off the disk has become radiatively efficient with $\epsilon_{\text{disk}} = 0.1$.

light of the on-axis orientation for the sample of jetted TDEs. Indeed, even low-luminosity AGN powering relatively weaker jets exhibit a positive disk-jet coupling correlation, albeit shallower than observed for powerful radio galaxies and quasars (Nagar et al. 2005; Su et al. 2016).

Our results suggest that jetted TDEs may preferentially form from lower mass black holes when compared to non-relativistic events which comprise the bulk of the TDE population and typically occur in galaxies hosting more massive black holes (Mockler et al. 2019; Ryu et al. 2020; Nicholl et al. 2022; Hammerstein et al. 2023), similar to the findings of Somalwar et al. 2023 based on a sample of radio-selected TDEs. If the latter form in systems with larger black hole masses, the paucity of jets may be a direct consequence of the lower jet efficiency and higher disk efficiency in this mass regime. Indeed, a positive correlation between black hole mass and disk radiative efficiency has been suggested in a sample of optically bright TDEs (Nicholl et al. 2022). At high black hole masses, such systems would therefore require extremely powerful jets (i.e., large jet efficiencies) to outshine their accretion disks.

3.3. Estimating the Mass of the Disrupting SMBH: Timescale of Jet Shut-off

Separate from the luminosity at jet shut-off, we can independently infer the mass of the disrupting SMBH from the *timescale* of jet shut-off. For a main-sequence star, the fallback accretion rate \dot{M} onto the BH peaks at a timescale $t \approx t_{\text{fb}}$ given by (e.g., Ulmer 1999):

$$t_{\text{fb}} = 0.11 \text{ yr} \left(\frac{M_{\text{BH}}}{10^6 M_{\odot}} \right)^{1/2} \left(\frac{M_{*}}{M_{\odot}} \right)^{-1} \quad (6)$$

and subsequently decays following a power law

$$\dot{M} = \dot{M}_{\text{peak}} (t/t_{\text{fb}})^{-\alpha} \quad (7)$$

where $\alpha = 5/3$ for a complete disruption and $\alpha = 2.2$ for a partial disruption in which the stellar core survives and $\lesssim 50\%$ of the stellar mass is accreted onto the black hole (Guillochon & Ramirez-Ruiz 2013). The Eddington ratio, $\lambda = \dot{M}/\dot{M}_{\text{Edd}}$, therefore evolves as

$$\lambda = \lambda_{\text{peak,fb}} (t/t_{\text{fb}})^{-\alpha}. \quad (8)$$

Assuming 100% efficiency in fallback mass reaching the black hole, the peak Eddington ratio is given by (Stone et al. 2013):

$$\lambda_{\text{peak,fb}} \simeq 133 \epsilon_{\text{disk,-1}} \left(\frac{\alpha-1}{2/3} \right) \left(\frac{M_{\text{BH}}}{10^6 M_{\odot}} \right)^{-3/2} \left(\frac{M_{*}}{M_{\odot}} \right)^2. \quad (9)$$

In reality, the accretion of matter onto the black hole is not a strictly efficient process (Metzger & Stone 2016) as some fraction of the initially bound stellar debris becomes

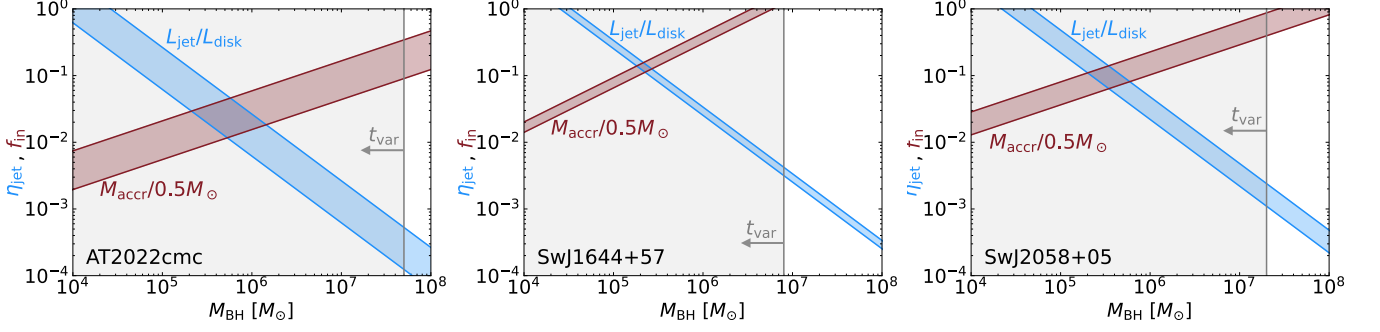


Figure 3. Allowed phase space of black holes masses as a function of both the jet efficiency ($\eta_{\text{jet}} = \epsilon_{\text{jet}}/\epsilon_{\text{disk}}$) and the fraction of accreted matter ($f_{\text{in}} = f_{\text{accr}} f_{\text{circ}} f_{\text{partial}}$) for AT2022cmc, SwJ1644+57, and SwJ2058+05 where individual curves correspond to the ratio of intrinsic jet and disk luminosity ($L_{\text{jet}}/L_{\text{disk}}$ with $L_{\text{jet}} = L_{\text{jet,off}} f_{\text{beam},200}^{-1} f_{\text{bol},3}$) at jet shut-off (blue curves) and the total accreted mass relative to a complete disruption ($M_{\text{accr}}/0.5M_{\odot}$; red curves). The width of each curve corresponds to the uncertainty in the X-ray luminosity and timescale of jet shut-off. For a given black hole mass, there exists a one-to-one mapping between f_{in} and η_{jet} . The gray shaded regions denotes the upper limit constraints on M_{BH} for each source from X-ray variability arguments.

unbound due to shocks formed at the self-intersection point of the debris stream (Lu & Bonnerot 2020). Moreover, the low gravitational binding energy of the debris, coupled with the fact that the infalling gas cannot radiatively cool when the fallback rate is super-Eddington (Strubbe & Quataert 2009), implies that only a small fraction of the disrupted stellar material is accreted by the black hole on a viscous timescale (Shen & Matzner 2014; Metzger & Stone 2016). We therefore parameterize the disk efficiency in converting the fallback accretion rate, given by eq. 8 and 9, into luminosity in terms of the fraction of accreted matter $f_{\text{in}} = f_{\text{accr}} f_{\text{circ}} f_{\text{partial}}$, where f_{accr} is the accretion efficiency, f_{circ} is the circularization efficiency, and f_{partial} accounts for a partial disruption in which only a fraction of stellar mass is stripped from the star. The Eddington ratio at the black hole is therefore given by:

$$\lambda_{\text{peak,BH}} = f_{\text{in}} \lambda_{\text{peak,fb}} \quad (10)$$

Taking $\lambda = 1$ to mark the transition from super- to sub-Eddington accretion and hence the point at which the jet shuts off, the jet shut-off time is given by:

$$t_{\text{off}} = t_{\text{fb}} \lambda_{\text{peak,BH}}^{1/\alpha} \quad (11)$$

Using equations 6, 9, 10, and 11 with $\alpha = 2.1$ as constrained from our MCMC analysis, our inferred jet shut-off time of $t_{\text{rest}} = 98$ days, and assuming a solar mass star, in Figure 3 we plot black hole mass as a function of f_{in} , where we adopt $\epsilon_{\text{disk}} = 0.1$ as a typical radiative efficiency.⁷ The result is a curve in the $f_{\text{in}} - M_{\text{BH}}$ phase-space corresponding to the fraction of accreted mass relative to a full disruption, where

⁷ In reality, the radiative efficiency for super-Eddington accretion disks decreases as the Eddington ratio λ increases (Jiang et al. 2019). For our purposes, and given that we carry out our calculations at the time of jet shut-off when the radiative efficiency is expected to be close to the typical value, we adopt a constant radiative efficiency $\epsilon_{\text{disk}} = 0.1$.

$f_{\text{in}} = 1$ implies a complete disruption in which $0.5 M_{\odot}$ is accreted onto the black hole.⁸

Given $L_{\text{jet,off}}$ and t_{off} , for fixed values of M_{BH} in Figure 3, there exist corresponding values of f_{in} and η_{jet} . Under the above supposition that the jet and disk luminosities are comparable (i.e. $\eta_{\text{jet}} \gtrsim 10^{-1}$), as in powerful blazars and radio-loud quasars, and $M_{\text{BH}} \lesssim 10^5 M_{\odot}$, f_{in} is constrained to $\lesssim 10^{-2}$ for AT2022cmc, implying a small fraction of total accreted mass relative to a complete disruption in which $0.5 M_{\odot}$ is accreted. This is consistent with the framework presented by Metzger & Stone 2016 in which they postulate that $f_{\text{in}} \ll 1$ is required to produce the observed outflows in TDEs. On the other hand, if the jet-disk coupling in TDEs is intrinsically distinct from that of AGN, the jet may be radiatively inefficient ($\eta_{\text{jet}} \lesssim 10^{-3}$) at high black hole masses ($M_{\text{BH}} \sim 10^7 M_{\odot}$) despite a large fraction of accreted mass ($f_{\text{in}} \gtrsim 0.1$). In other words, the X-ray luminosity would represent a small fraction of the total energy budget of the system. Such a scenario may arise due to differences in the available magnetic reservoir for TDEs (Kellely et al. 2014), for example, or if a large fraction of jets are choked (Lu et al. 2023; Teboul & Metzger 2023) or launched off-axis (Dai et al. 2018). Indeed, the latter scenario may be reflected by the smaller fraction of relativistic jetted TDEs relative to the fraction of radio-quiet quasars (Alexander et al. 2020).

⁸ Here we assume the tidal disruption of a $1 M_{\odot}$ main sequence star in which half of the stellar material is unbound from the system as the most plausible scenario and additionally allow for the possibility that the star is only partially disrupted. In the case of a white dwarf disruption, which is tenable for a $10^5 M_{\odot}$ black hole and indeed was suggested for Sw J1644+57 based on the short timescale variability in the *Swift*/XRT lightcurve (Krolik & Piran 2011), in which the radius and mass of the star are inversely related ($r_* \propto M_*^{-1/3}$), the mass accretion rate on the same timescale is approximately 10^3 times smaller (Tchekhovskoy et al. 2014), implying a larger accreted mass fraction for a fixed black hole mass.

Adopting the same methodology for Sw J1644+57⁹ and Sw J2058+05¹⁰, we trace out similar regions in the $f_{\text{in}} - M_{\text{BH}}$ phase-space in Figure 3. We note that in both cases, the timescale of jet shut-off occurs a factor of two to four times later than in AT2022cmc; requiring the same condition of $\eta_{\text{jet}} \gtrsim 10^{-1}$ therefore allows for somewhat larger black hole masses relative to AT2022cmc of $\sim \text{a few} \times 10^5 M_{\odot}$ and hence a larger fraction of accreted mass $f_{\text{in}} \lesssim 0.1$, implying that the total accreted mass in these systems is more comparable to that of a complete disruption.

3.4. Comparison to Other SMBH Mass Estimates

We compare our SMBH mass estimates for AT2022cmc and other jetted TDEs as derived from the jet shut-off time and X-ray luminosity to estimates derived via other methods. First, we use the observed variability in the X-ray light curves at early times to place an upper limit on the mass of the SMBH. In particular, we can equate the size of the X-ray emitting region r_s to the Schwarzschild radius of a black hole with mass M_{BH} . For an observed variability timescale $t_{\text{var,sec}} \sim r_s/c$ in seconds, the mass of the SMBH is given by

$$M_{\text{BH}} \lesssim 10^5 M_{\odot} \frac{t_{\text{var,sec}}}{(1+z)} \quad (12)$$

In the case of AT2022cmc, X-ray variability is observed over a wide range of timescales spanning 1000 s to \sim days. We adopt a minimum variability timescale $t_{\text{var}} = 1000$ s (Pasham et al. 2023). The resulting limit on the SMBH mass for AT2022cmc is $M_{\text{BH}} \lesssim 5 \times 10^7 M_{\odot}$.

For Sw J1644+57, the early time X-ray light curve out to $t_{\text{obs}} \approx 10$ days is punctuated by rapid variability on timescales as short as ~ 100 s (Mangano et al. 2016). We therefore constrain the black hole mass for Sw J1644+57 based on variability arguments to $M_{\text{BH}} \lesssim 8 \times 10^6 M_{\odot}$, as in Burrows et al. (2011). Conversely, the putative detection of quasi-periodic oscillations (QPOs) in the X-ray light curve of Sw J1644+57 (Reis et al. 2012) enabled constraints on the black hole mass of $10^5 - 10^6 M_{\odot}$ (Abramowicz & Liu 2012), comparable to the black holes mass we infer in our jet shut-off paradigm. For Sw J1112–82, the X-ray light curve exhibited variability on timescales of a few thousand seconds (Brown et al. 2015), corresponding to a limit on the SMBH mass of $\lesssim 2 \times 10^7 M_{\odot}$. Finally, for Sw J2058+05, the observed variability timescale of ~ 500 s constrains the SMBH mass to $\lesssim 2 \times 10^8 M_{\odot}$. This is above the maximum allowed mass for TDEs of $< 10^8 M_{\odot}$, above which the disruption radius lies within the Schwarzschild radius and the star is thus swallowed whole (Rees 1988), and hence is not constraining.

⁹ We adopt $\alpha = 5/3$ for Sw J1644+57, consistent with its observed X-ray light curve (Burrows et al. 2011).

¹⁰ We constrain the timescale of jet shut-off and the power-law index for Sw J2058+05 in Appendix A.

Finally, we note that several limits have been placed on the SMBH mass for jetted TDEs using the galaxy bulge – black hole mass relation (McConnell & Ma 2013). In the case of AT2022cmc, the host galaxy is not detected in deep ground-based imaging with the Canada-French-Hawaii Telescope down to a limiting r -band magnitude of 24.5 (3σ), corresponding to an upper limit on the host galaxy mass of $< 1.6 \times 10^{11} M_{\odot}$ and hence an SMBH mass of $M_{\text{BH}} < 4.7 \times 10^8 M_{\odot}$ (Andreoni et al. 2022a). Similarly derived constraints for Sw J1644+57 and Sw J2058+05 have led to SMBH mass limits of $M_{\text{BH}} < 2 \times 10^7 M_{\odot}$ (Burrows et al. 2011) and $M_{\text{BH}} < 3 \times 10^7 M_{\odot}$ (Pasham et al. 2015), respectively. For Sw J1112-82, Brown et al. (2015) obtain an SMBH mass limit of $2 \times 10^6 M_{\odot}$ using the black hole mass – bulge mass relation of Häring & Rix (2004).

In general, we find that our SMBH mass estimates as inferred from the timescale and luminosity of jet shut-off are consistent with estimates derived via other methods, but that such methods do not sufficiently probe the low mass regime where our models are favored.

3.5. Constraining the Mass Accretion Rate and the Total Accreted Mass

While the precise nature of relativistic jet production in TDEs is not well understood, such jets are canonically expected to form when the accretion rate onto the black hole exceeds the Eddington rate (Giannios & Metzger 2011). The low occurrence rate of jetted TDEs however suggests that super-Eddington accretion, which is expected at early times for disruptions of solar mass stars by black holes with $M_{\text{BH}} \lesssim 10^8 M_{\odot}$ (De Colle et al. 2012), is not a sufficient condition for powering relativistic jets, and that additional parameters such as black hole spin or disk-jet alignment must play a role (Stone & Loeb 2012; Tchekhovskoy et al. 2014; Franchini et al. 2016; Curd & Narayan 2019; Zanazzi & Lai 2019; Teboul & Metzger 2023). Nevertheless, the rapid drop in flux observed in the X-ray light curves of jetted TDEs on timescales commensurate with a transition to sub-Eddington accretion as seen in numerical simulations supports a connection between super-Eddington accretion and jet production (De Colle et al. 2012).

With the inference that the accretion rate at $t_{\text{rest}} = 100$ days is equal to the Eddington accretion rate, we can estimate the total accreted mass onto the SMBH for AT2022cmc. First, we calculate the Eddington accretion rate assuming L_{Edd} is equal to the isotropic X-ray luminosity at the time of jet shut-off ($L_X \approx 10^{44} \text{ erg s}^{-1}$) and adopting a beaming angle of 0.1 rad and a bolometric correction factor of 3 as before. We find $\dot{M}(100 \text{ days}) \approx \dot{M}_{\text{Edd}} \approx 0.003 M_{\odot} \text{ yr}^{-1}$ for a radiative efficiency $\epsilon_{\text{disk}} = 0.1$. Following the prescription of Zauderer et al. (2013), a simple model for the mass accretion rate is given by $\dot{M}(t) = \dot{M}_p (t/t_j)^{-\alpha}$, where \dot{M}_p is the peak accretion

rate and t_j is the timescale over which the X-ray luminosity is constant. We take $t_j = 2.5$ days given the onset of observable X-ray emission on this timescale and the lack of a plateau in the X-ray light curve (Andreoni et al. 2022a; Pasham et al. 2023) and $\alpha = 2.1$ and find $\dot{M}_p \approx 4.6 M_\odot \text{ yr}^{-1}$. Integrating the mass accretion rate out to $t_{\text{off}} = 100$ days where $\dot{M}(t) = \dot{M}_p$ at $t < 2.5$ days and $\dot{M}(t) = \dot{M}_p(t/t_j)^{-2.1}$ at $t \gtrsim 2.5$ days, we find a total accreted mass of $\approx 0.1 M_\odot$.

Our estimate of the total accreted mass is larger than inferred from Figure 3, where $M_{\text{BH}} \sim 10^5 M_\odot$ implies a total accreted mass $M_{\text{accr}} \sim f_{\text{in}} \times 0.5 M_\odot \approx 10^{-2} \times 0.5 M_\odot \approx 0.01 M_\odot$. However, as discussed in Section 3.3, in Figure 3, we account for additional efficiency factors ($f_{\text{in}} = f_{\text{accr}} f_{\text{circ}} f_{\text{partial}}$) for converting the fallback accretion into luminosity, which we neglect in our above calculation. Moreover, we consider our above estimate of $0.1 M_\odot$ approximate, given uncertainties in the assumed radiative efficiency which depends on the spin of the black hole (e.g., Novikov & Thorne 1973; Shakura & Sunyaev 1973; Sądowski & Narayan 2016). Similarly, if the jet instead shuts off at a fraction of the Eddington accretion rate (e.g., Tchekhovskoy et al. 2014), the total accreted mass will decrease linearly with this fraction. We thus consider our two independent estimates of the total accreted mass as broadly consistent with one another.

We repeat the above calculations for Sw J1644+57 and Sw J2058+05 adopting the same beaming and bolometric correction factors of 0.1 rad and 3, respectively. For Sw J1644+57, we take $t_j = 15$ days in the observer frame based on the observed X-ray plateau (Burrows et al. 2011) and $\alpha = 5/3$ and find a peak accretion rate of $\dot{M}_{\text{peak}} \sim 2.4 M_\odot \text{ yr}^{-1}$. The accretion rate at $t \lesssim 15$ days is therefore given by $\dot{M}(t) = \dot{M}_p$ and $\dot{M}(t) = \dot{M}_p(t/t_j)^{-5/3}$ at $t \gtrsim 15$ days. Integrating the mass accretion rate out to $t_{\text{off}} \approx 370$ days (rest-frame), the total accreted mass is $\approx 0.17 M_\odot$, consistent with the results of Zauderer et al. (2013). For Sw J2058+05, we adopt $t_j = 11$ days (Cenko et al. 2012) and $\alpha = 2.1$ and find $\dot{M}_p = 3.5 M_\odot \text{ yr}^{-1}$. The total mass accreted out to $t_{\text{off}} \approx 212$ days (rest-frame) is therefore $\approx 0.2 M_\odot$.

3.6. Revival of the Jet

As the fallback accretion rate continues to decline following $\dot{M} \propto t^{-2.1}$ and eventually reaches a few percent of Eddington, the disk is expected to transition to a radiatively inefficient advection-dominated accretion flow (Maccarone 2003), analogous to the “low/hard” state in X-ray binaries (Fender et al. 2004; Russell et al. 2011). At this point, the jet is expected to turn back on. Based on the Eddington accretion rate derived in Section 3.5, we estimate that the mass accretion rate will reach 2% Eddington at $t_{\text{obs}} \approx 3-5$ years (or $t_{\text{obs}} \approx 5-9$ years if instead the mass accretion rate more closely follows $\dot{M} \propto t^{-5/3}$) with an associated X-ray flux of $F_X \approx 1-5 \times 10^{-16} \text{ erg cm}^{-2} \text{ s}^{-1}$. As this is beyond the

detection limits of current X-ray facilities with reasonable exposure times, we conclude that continued X-ray monitoring of AT2022cmc is unlikely to detect a revival of the jetted emission, unless the transition to a “low/hard” state occurs at a larger fraction of the Eddington accretion rate. On the other hand, such a revival may be accompanied by a rapid rise in radio flux from the forward shock interaction of the jet with the ambient medium. Indeed, late-time radio rebrightening has been observed in a large fraction ($\sim 40\%$) of optically-selected TDEs (Horesh et al. 2021b; Cendes et al. 2023), although the underlying mechanism governing the rebrightening, as well as whether the mechanism is the same for all TDEs, remains unclear.

While jets have not been observed to turn back on for the existing sample of relativistic TDEs, late-time *Chandra* observations of Sw J1644+57 have detected faint X-rays consistent with emission from the expanding forward shock (Zauderer et al. 2013; Levan et al. 2016; Eftekhari et al. 2018). X-ray observations of AT2022cmc at late times, coupled with an extrapolation of the radio SED into the X-ray regime, will probe such emission and enable constraints on the synchrotron cooling frequency. Finally, we note that the detection of quiescent X-ray emission from a pre-existing low-luminosity AGN is unlikely, given the distance to AT2022cmc and expected luminosities for low-luminosity AGN of $L_X \lesssim 10^{42} \text{ erg s}^{-1}$ (Brusa et al. 2007).

4. CONCLUSIONS

We have presented late-time X-ray observations of AT2022cmc, the fourth relativistic TDE discovered to date. Our observations reveal a drop in the X-ray emission at $t_{\text{rest}} \approx 100$ days, which we attribute to the relativistic jet turning off, marking the third TDE for which such a transition is observed. Our main findings can be summarized as follows:

- We constrain the timescale of jet shut-off for AT2022cmc to $t_{\text{rest}} \approx 98_{-26}^{+38}$ days. Compared to other jetted TDEs, the relativistic jet powering AT2022cmc shuts off a factor of two to four times earlier in the rest-frame, while the X-ray luminosities at shut-off (and hence Eddington luminosities) are comparable across all three events. The X-ray light curve prior to jet shut-off decays following $t^{-2.1}$, possibly indicative of a partial stellar disruption.
- From the X-ray luminosity and timescale of jet shutoff, we parameterize the black hole mass in terms of the jet efficiency (η_{jet}) and fraction of accreted matter (f_{in}), and find that lower black hole masses of $\lesssim 10^5 M_\odot$, where the disk and jet luminosities are comparable and the fraction of accreted mass is low, are favored. We find similar, albeit somewhat larger black hole masses of \lesssim a few $\times 10^5 M_\odot$ for Sw J1644+57 and Sw J2058+05,

which we suggest may imply that jetted TDEs preferentially form in lower mass black hole systems than non-relativistic events (e.g., Hammerstein et al. 2023) where the jet efficiency is low, and the corresponding disk efficiency is high (Nicholl et al. 2022).

- We find that the overall accreted mass by $t_{\text{off}} \approx 100$ days (rest-frame) is $\approx 0.1 M_{\odot}$, and the peak accretion rate is $\dot{M}_p \sim 4.6 M_{\odot} \text{ yr}^{-1}$. This is comparable to estimates of the total accreted mass for both Sw J1644+57 and Sw J2058+05.
- We predict that the jet associated with AT2022cmc will reach an accretion rate of 2% Eddington and turn back on around $t_{\text{obs}} \approx 3 - 9$ years depending on the mass fallback rate. However, the associated X-ray flux on this timescale of $F_X \approx 1 - 5 \times 10^{-16} \text{ erg cm}^{-2} \text{ s}^{-1}$ precludes a detection with present-day X-ray facilities.

While we attribute the sudden drop in X-ray emission for AT2022cmc to an accretion state transition, we note that sev-

eral alternative models in which the jet becomes misaligned with our line of sight can reconcile the abrupt termination of X-rays in TDEs on timescales of \sim years post-disruption. One such mechanism is the Bardeen-Petterson effect, in which the outer accretion disk is held tilted relative to the inner disk leading to a warped disk (Bardeen & Petterson 1975). Such a warp may induce a reorientation of the jet out of our line of sight (Liska et al. 2021; Chatterjee et al. 2023). Alternatively, the disk can be tilted due to stream self-intersections (Curd et al. 2023). As the self-intersection outflow weakens, the density contrast between the TDE stream and the disk increases resulting in a rapid realignment of the jet with the disk and an abrupt dropoff in the observed X-ray luminosity.

As optical surveys contribute to an increasing rate of detections for jetted TDEs, X-ray monitoring on \sim year timescales will enable constraints on the jet shut-off time for a larger sample of events and facilitate measurements of the SMBH mass function for relativistic TDEs.

APPENDIX

A. CONSTRAINING THE JET SHUT-OFF TIME IN SW J2058+05

While the X-ray light curve of Sw J2058+05 (Figure 4) exhibits a rapid decline following an earlier $\sim t^{-2}$ decay (Pasham et al. 2015) attributable to the cessation of jet activity, as in the case of AT2022cmc, the precise timescale of jet-shutoff is not well-constrained given the sparse sampling of the X-ray light curve on this timescale. We therefore apply the above MCMC prescription to constrain the jet shut-off time for Sw J2058+05. We fit the light curve beginning at $t_{\text{rest}} \approx 12$ days to account for the plateau in the X-ray light curve at $t \lesssim 12$ days. As in the case of AT2022cmc, we adopt log-uniform priors for F_X and t_{off} , and allow for t_{off} to span the full timescale of the X-ray light curve ($t \sim 0 - 410$ days). We use linearly uniform priors for the power law indices, with $-10 < \alpha_1 < 0$ and $-50 < \alpha_2 < -5$. We sample the posterior distributions using 1000 Markov chains and 30000 steps, and discard the first 3000 steps ($\approx 6 \times$ the autocorrelation length). We find an acceptance fraction of 0.36. From our MCMC analysis, we constrain the jet shut-off time in Sw J2058+05 to $t_{\text{rest}} = 212_{-35}^{+46}$ days ($t_{\text{obs}} \approx 460$ days).

ACKNOWLEDGMENTS

The scientific results reported in this article are based on observations made by the *Chandra X-ray Observatory* under program GO 24700310, PI: Eftekhari. T. E. is supported by NASA through the NASA Hubble Fellowship grant HST-HF2-51504.001-A awarded by the Space Telescope Science Institute, which is operated by the Association of Universities for Research in Astronomy, Inc., for NASA, under contract NAS5-26555. A. T. acknowledges support by NSF AST-2009884, AST-2107839, AST-1815304, AST-1911080, OAC-2031997, AST-2206471 and NASA 80NSSC22K0031 and 80NSSC21K1746 grants. K. D. A. acknowledges support provided by the NSF through award AST-2307668.

Facilities: *Chandra X-ray Observatory*

Software: `Astropy` (Astropy Collaboration et al. 2013, 2018, 2022), `matplotlib` (Hunter 2007), `numpy` (Harris et al. 2020), `SAOImageDS9` (Joye & Mandel 2003), `scipy` (Virtanen et al. 2020), `CIAO` (v4.13) (Fruscione et al. 2006),

REFERENCES

- Abramowicz, M. A., & Liu, F. K. 2012, *A&A*, 548, A3
- Alexander, K. D., van Velzen, S., Horesh, A., & Zauderer, B. A. 2020, *SSRv*, 216, 81

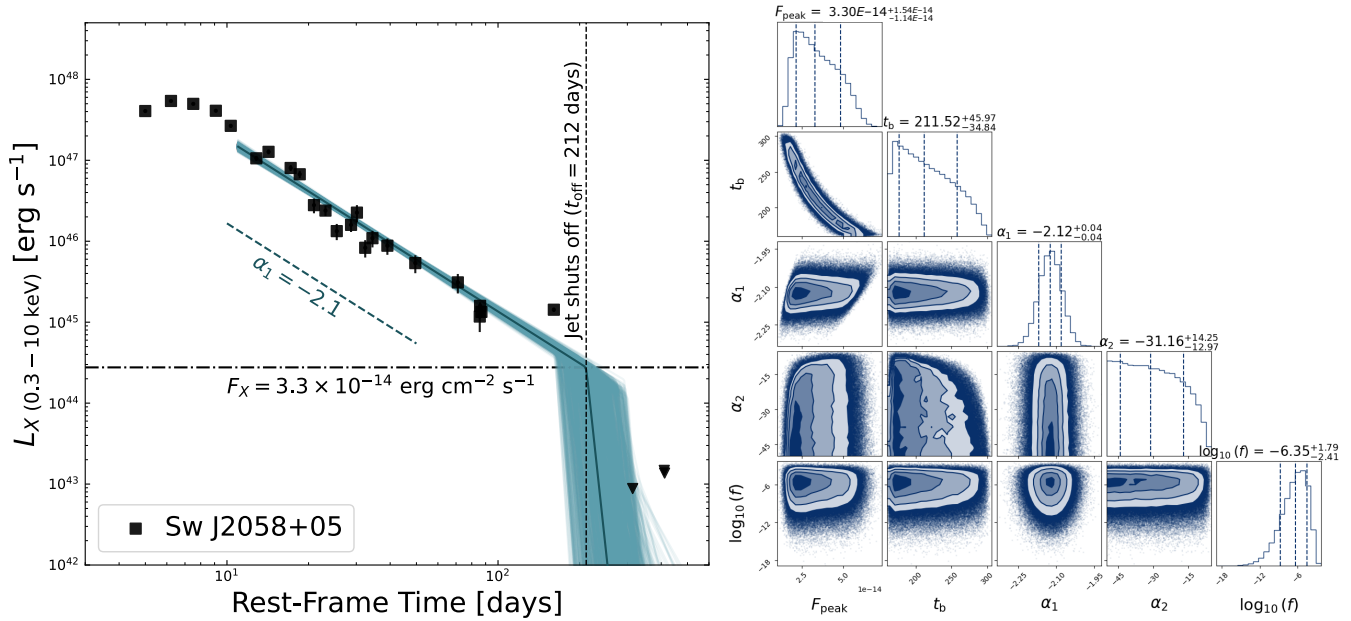


Figure 4. **Left:** X-ray light curve of Sw J2058+05 (Pasham et al. 2015; black squares) with our best fit broken power-law model (dark blue curve) which indicates a jet shut-off time of $t_{\text{rest}} \approx 212_{-35}^{+46}$ days. The X-ray light curve prior to the jet shut-off decays following $t^{-2.1}$. **Right:** Results from our MCMC parameter estimation for a broken power law fit to the X-ray light curve of Sw J2058+05. Marginalized posterior distributions for each parameter are shown on the diagonal, where dashed lines indicate the median and 68% confidence interval.

Andreoni, I., Coughlin, M. W., Perley, D. A., et al. 2022a, *Nature*, **612**, 430

Andreoni, I., Coughlin, M., Ahumada, T., et al. 2022b, GRB Coordinates Network, **31590**, 1

Astropy Collaboration, Robitaille, T. P., Tollerud, E. J., et al. 2013, *A&A*, **558**, A33

Astropy Collaboration, Price-Whelan, A. M., Sipőcz, B. M., et al. 2018, *AJ*, **156**, 123

Astropy Collaboration, Price-Whelan, A. M., Lim, P. L., et al. 2022, *ApJ*, **935**, 167

Auchettl, K., Ramirez-Ruiz, E., & Guillochon, J. 2018, *ApJ*, **852**, 37

Bardeen, J. M., & Petterson, J. A. 1975, *ApJL*, **195**, L65

Berger, E., Zauderer, A., Pooley, G. G., et al. 2012, *ApJ*, **748**, 36

Blandford, R. D., & Znajek, R. L. 1977, *MNRAS*, **179**, 433

Bloom, J. S., Giannios, D., Metzger, B. D., et al. 2011, *Science*, **333**, 203

Bonnerot, C., Price, D. J., Lodato, G., & Rossi, E. M. 2017, *MNRAS*, **469**, 4879

Brown, G. C., Levan, A. J., Stanway, E. R., et al. 2015, *MNRAS*, **452**, 4297

Brusa, M., Zamorani, G., Comastri, A., et al. 2007, *ApJS*, **172**, 353

Burrows, D. N., Kennea, J. A., Ghisellini, G., et al. 2011, *Nature*, **476**, 421

Cendes, Y., Berger, E., Alexander, K. D., et al. 2023, *arXiv e-prints*, [arXiv:2308.13595](https://arxiv.org/abs/2308.13595)

Cenko, S. B., Krimm, H. A., Horesh, A., et al. 2012, *ApJ*, **753**, 77

Chatterjee, K., Liska, M., Tchekhovskoy, A., & Markoff, S. 2023, *arXiv e-prints*, [arXiv:2311.00432](https://arxiv.org/abs/2311.00432)

Coughlin, E. R., & Nixon, C. J. 2019, *ApJL*, **883**, L17

Curd, B., Anantua, R., West, H., & Duran, J. 2023, *arXiv e-prints*, [arXiv:2310.20592](https://arxiv.org/abs/2310.20592)

Curd, B., & Narayan, R. 2019, *MNRAS*, **483**, 565

Dai, J. L., Lodato, G., & Cheng, R. 2021, *SSRv*, **217**, 12

Dai, L., McKinney, J. C., Roth, N., Ramirez-Ruiz, E., & Miller, M. C. 2018, *ApJL*, **859**, L20

De Colle, F., Guillochon, J., Naiman, J., & Ramirez-Ruiz, E. 2012, *ApJ*, **760**, 103

De Colle, F., & Lu, W. 2020, *NewAR*, **89**, 101538

Eftekhari, T., Berger, E., Zauderer, B. A., Margutti, R., & Alexander, K. D. 2018, *ApJ*, **854**, 86

Fender, R. P., Belloni, T. M., & Gallo, E. 2004, *MNRAS*, **355**, 1105

Foreman-Mackey, D., Hogg, D. W., Lang, D., & Goodman, J. 2013, *PASP*, **125**, 306

Franchini, A., Lodato, G., & Facchini, S. 2016, *MNRAS*, **455**, 1946

Fruscione, A., McDowell, J. C., Allen, G. E., et al. 2006, in Society of Photo-Optical Instrumentation Engineers (SPIE) Conference Series, Vol. 6270, Society of Photo-Optical Instrumentation Engineers (SPIE) Conference Series, ed. D. R. Silva & R. E. Doxsey, 62701V

Gehrels, N. 1986, *ApJ*, **303**, 336

Gelman, A., Roberts, G. O., & Gilks, W. R. 1996, in Bayesian Statistics, ed. J. M. Bernardo, J. O. Berger, A. P. Dawid, & A. F. M. Smith (Oxford University Press, Oxford)

- Ghisellini, G., Tavecchio, F., Foschini, L., et al. 2010, *MNRAS*, **402**, 497
- Giannios, D., & Metzger, B. D. 2011, *MNRAS*, **416**, 2102
- Guillochon, J., & McCourt, M. 2017, *ApJL*, **834**, L19
- Guillochon, J., & Ramirez-Ruiz, E. 2013, *ApJ*, **767**, 25
- Hammerstein, E., van Velzen, S., Gezari, S., et al. 2023, *ApJ*, **942**, 9
- Häring, N., & Rix, H.-W. 2004, *ApJL*, **604**, L89
- Harris, C. R., Millman, K. J., van der Walt, S. J., et al. 2020, *Nature*, **585**, 357
- Helsel, D. R. 2005, *Environmental Science and Technology*, **39**, 419A
- Horesh, A., Cenko, S. B., & Arcavi, I. 2021a, *Nature Astronomy*, **5**, 491
- Horesh, A., Sfaradi, I., Fender, R., et al. 2021b, *ApJL*, **920**, L5
- Hunter, J. D. 2007, *Computing in Science and Engineering*, **9**, 90
- Inoue, Y., Doi, A., Tanaka, Y. T., Sikora, M., & Madejski, G. M. 2017, *ApJ*, **840**, 46
- Jiang, Y.-F., Stone, J. M., & Davis, S. W. 2019, *ApJ*, **880**, 67
- Joye, W. A., & Mandel, E. 2003, in *Astronomical Society of the Pacific Conference Series*, Vol. 295, *Astronomical Data Analysis Software and Systems XII*, ed. H. E. Payne, R. I. Jedrzejewski, & R. N. Hook, 489
- Kalberla, P. M. W., Burton, W. B., Hartmann, D., et al. 2005, *A&A*, **440**, 775
- Kelley, L. Z., Tchekhovskoy, A., & Narayan, R. 2014, *MNRAS*, **445**, 3919
- Krolik, J. H., & Piran, T. 2011, *ApJ*, **743**, 134
- Krolik, J. H., & Piran, T. 2012, *ApJ*, **749**, 92
- Laskar, T., Berger, E., Tanvir, N., et al. 2014, *ApJ*, **781**, 1
- Lawless, J. F. 2002, *Statistical Models and Methods for Lifetime Data* (Wiley)
- Levan, A. J., Tanvir, N. R., Cenko, S. B., et al. 2011, *Science*, **333**, 199
- Levan, A. J., Tanvir, N. R., Brown, G. C., et al. 2016, *ApJ*, **819**, 51
- Liska, M., Hesp, C., Tchekhovskoy, A., et al. 2021, *MNRAS*, **507**, 983
- Lu, W., & Bonnerot, C. 2020, *MNRAS*, **492**, 686
- Lu, W., Matsumoto, T., & Matzner, C. D. 2023, *arXiv e-prints*, [arXiv:2310.15336](https://arxiv.org/abs/2310.15336)
- Maccarone, T. J. 2003, *A&A*, **409**, 697
- Mangano, V., Burrows, D. N., Sbarufatti, B., & Cannizzo, J. K. 2016, *ApJ*, **817**, 103
- McConnell, N. J., & Ma, C.-P. 2013, *ApJ*, **764**, 184
- Metzger, B. D., & Stone, N. C. 2016, *MNRAS*, **461**, 948
- Mockler, B., Guillochon, J., & Ramirez-Ruiz, E. 2019, *ApJ*, **872**, 151
- Nagar, N. M., Falcke, H., & Wilson, A. S. 2005, *A&A*, **435**, 521
- Nicholl, M., Lanning, D., Ramsden, P., et al. 2022, *MNRAS*, **515**, 5604
- Novikov, I. D., & Thorne, K. S. 1973, in *Black Holes (Les Astres Occlus)*, 343–450
- Pasham, D. R., Cenko, S. B., Levan, A. J., et al. 2015, *ApJ*, **805**, 68
- Pasham, D. R., Lucchini, M., Laskar, T., et al. 2023, *Nature Astronomy*, **7**, 88
- Piran, T., Sądowski, A., & Tchekhovskoy, A. 2015, *MNRAS*, **453**, 157
- Planck Collaboration, Aghanim, N., Akrami, Y., et al. 2020, *A&A*, **641**, A6
- Rees, M. J. 1988, *Nature*, **333**, 523
- Reis, R. C., Miller, J. M., Reynolds, M. T., et al. 2012, *Science*, **337**, 949
- Rhodes, L., Bright, J. S., Fender, R., et al. 2023, *MNRAS*, **521**, 389
- Russell, D. M., Miller-Jones, J. C. A., Maccarone, T. J., et al. 2011, *ApJL*, **739**, L19
- Ryu, T., Krolik, J., & Piran, T. 2020, *ApJ*, **904**, 73
- Sari, R., Piran, T., & Halpern, J. P. 1999, *ApJL*, **519**, L17
- Sato, Y., Murase, K., Bhattacharya, M., et al. 2024, *arXiv e-prints*, [arXiv:2404.13326](https://arxiv.org/abs/2404.13326)
- Saxton, C. J., Soria, R., Wu, K., & Kuin, N. P. M. 2012, *MNRAS*, **422**, 1625
- Sfaradi, I., Beniamini, P., Horesh, A., et al. 2024, *MNRAS*, **527**, 7672
- Shakura, N. I., & Sunyaev, R. A. 1973, *A&A*, **24**, 337
- Shen, R.-F., & Matzner, C. D. 2014, *ApJ*, **784**, 87
- Sądowski, A., & Narayan, R. 2016, *MNRAS*, **456**, 3929
- Somalwar, J. J., Ravi, V., Dong, D. Z., et al. 2023, *arXiv e-prints*, [arXiv:2310.03791](https://arxiv.org/abs/2310.03791)
- Stone, N., & Loeb, A. 2012, *Physical Review Letters*, **108**
- Stone, N., Sari, R., & Loeb, A. 2013, *MNRAS*, **435**, 1809
- Stone, N. C., Vasiliev, E., Kesden, M., et al. 2020, *SSRv*, **216**, 35
- Strubbe, L. E., & Quataert, E. 2009, *MNRAS*, **400**, 2070
- Su, R., Liu, X., & Zhang, Z. 2016, *Astrophysics and Space Science*, **362**
- Sun, H., Zhang, B., & Li, Z. 2015, *ApJ*, **812**, 33
- Tanvir, N. R., de Ugarte Postigo, A., Izzo, L., et al. 2022, *GRB Coordinates Network*, **31602**, 1
- Tchekhovskoy, A., Metzger, B. D., Giannios, D., & Kelley, L. Z. 2014, *MNRAS*, **437**, 2744
- Teboul, O., & Metzger, B. D. 2023, *ApJL*, **957**, L9
- Ulmer, A. 1999, *ApJ*, **514**, 180
- Virtanen, P., Gommers, R., Oliphant, T. E., et al. 2020, *Nature Methods*, **17**, 261
- Wang, X.-G., Zhang, B., Liang, E.-W., et al. 2018, *ApJ*, **859**, 160
- Yao, Y., Lu, W., Harrison, F., et al. 2024, *ApJ*, **965**, 39
- Zanazzi, J. J., & Lai, D. 2019, *MNRAS*, **487**, 4965
- Zauderer, B. A., Berger, E., Margutti, R., et al. 2013, *ApJ*, **767**, 152
- Zauderer, B. A., Berger, E., Soderberg, A. M., et al. 2011, *Nature*, **476**, 425